Pore-network simulations of two-phase flow in a thin porous layer of mixed wettability: Application to water transport in gas diffusion layers of proton exchange membrane fuel cells

S. Pulloor Kuttanikkad [a,b,c], M. Prat [b,c,*], J. Pauchet [a]

[a] CEA, LITEN, LCPEM, F-38054 Grenoble, France
[b] Université de Toulouse, INPT, UPS, IMFT, Avenue Camille Soula 31400, Toulouse, France
[c] CNRS, IMFT 31400, Toulouse, France

ARTICLE INFO

ABSTRACT

Pore network simulations are performed to study water transport in a model gas diffusion layer (GDL) of polymer electrolyte membrane fuel cells (PEMFCs) in relation with the change in hydrophobicity that might be due to aging or temperature effect. The change in hydrophobicity is taken into account by changing randomly the fraction of hydrophilic elements, pores or throats, in the network. The transport and equilibrium properties of the model GDL are computed as a function of liquid saturation as well as at breakthrough varying the fraction of hydrophilic elements. The results indicate that the hydrophilic element percolation threshold marks the transition between two domains. The system is found to be weakly dependent on the fraction of hydrophilic elements as long as this fraction is below the percolation threshold whereas an increase in wettability above the percolation threshold favours a greater blockage of the pore space by the water and therefore a diminished access of gas to the catalyst layer. This model may help assess the effect of a change in wettability on the fuel cell performance and may also help suggest better GDL designs in relation with the water management problem in PEMFCs.

© 2010 Elsevier B.V. All rights reserved.

1. Introduction

Water management continues to be a major issue for proton exchange membrane fuel cells, e.g. [1] and references therein, and it is now clear that the gas diffusion layer (GDL) is an important element in the prospect of a better water management. Optimizing a GDL for the water management problem is, loosely, having enough water to ensure the good hydration of the electrolyte while minimizing the impact of liquid water in the pores on the gas access to the catalyst layer. Despite numerous studies devoted to GDL, e.g. [2] and references therein, there is still no obvious way of optimizing the fuel cell performances by playing with the GDL properties. One reason is that the effect of GDL wettability properties is still not fully well understood. Pore network simulations, e.g. [3], suggest that a sufficiently hydrophobic GDL is better than a hydrophilic one. This is because water invasion in a hydrophobic porous medium in the quasi-static limit that is expected to prevail for flows in fuel cells leads to capillary fingering whereas the invasion pattern is compact in a hydrophilic medium. The capillary

fingering pattern leaves many pores not invaded by the liquid and therefore available for the gas transport. In contrast, the compact invasion pattern blocks rapidly the gas transport across the GDL. This sounds consistent with the fact that a GDL is generally treated with a hydrophobic fluoropolymer. However, the distribution of the fluoropolymer on the carbon fibres forming the GDL microstructure is heterogeneous, e.g. [1] and references therein. The SEM micrographs of GDL reported in [1] indicate that there are more fluoropolymer at the junctions between fibres for example and that other parts of the fibres might be not coated by the fluoropolymer. However the more precise ToF-SIMS images also reported in [1] lead to the conclusion that the fluoropolymer is in fact present everywhere on the pore wall. Hence Teflon would be present in the form of thin films even in the regions of the microstructure which appear as seemingly not teflonized in the SEM micrographs. Since wetting is generally dominated by the top few monolayers of a surface [4], it is anticipated that the wetting properties of a teflonized GDL microstructure are uniform and close to the ones of water on Teflon. This leaves us with two options. The first option is to consider, as suggested in [1] as well as in [5], that the teflonization process is effective and therefore that the wettability of a GDL is spatially uniform, that is the (advancing) contact angle varies locally within a quite narrow range around 115° or possibly more. The second option, considered for example in [6–9], is to

* Corresponding author at: IMFT, Avenue Camille Soula 31400, Toulouse, France.
Tel.: +33 56134322883; fax: +33 56134322899.
 E-mail address: prat@imft.fr (M. Prat).

consider that a GDL should be envisioned as a system of mixed wettability, that is some regions of the microstructure are hydrophilic (with the local contact angle θ expected to be on the order of that of water on carbon, $\theta \sim 80°$) whereas others are hydrophobic, i.e. coated with the fluoropolymer. How to distribute the hydrophilic and hydrophobic regions on the pore wall surface is not obvious since we do not know for example the size of the hydrophilic (resp. hydrophobic) regions. As for example in [6], the simple option considered in this paper is to suppose that a fraction f of the pores is hydrophilic, the others (corresponding to the fraction $1 − f$) being hydrophobic and to explore the influence of f on water invasion or water distribution in the network. It could be argued that it is somewhat not consistent to consider mixed wettability systems since the recent results presented in [1,5] indicate that it seems more appropriate to assume a uniform wettability. It is shown, however, that our mixed wettability model is in good agreement with the most recent measurements of the capillary pressure curve. Thus it cannot be readily concluded from these measurements that the GDL is of uniform wettability. Even if the assumption of spatially uniform wettability is the correct assumption for the current teflonized GDLs, it remains interesting, anyway, to explore whether systems of mixed wettability would be better for the water management issue. Also, it is widely admitted that the GDLs lose hydrophobicity during the course of a PEMFC lifetime, e.g. [10]. It is unclear, however, whether this change in hydrophobicity occurs everywhere within the pore space or rather according to a scenario where the change in hydrophobicity would be due to the increase in the fraction of pore wall surface becoming hydrophilic over time. Also, it has been reported that a GDL tends to become more hydrophilic after exposure to liquid water at temperatures representative of the PEMFC operating conditions [11,12]. Increasing the fraction of hydrophilic pores in a mixed wettability model is a convenient way to explore the consequences of this change in wettability. As shown in [3], see also [13] and references therein, it is possible to explore numerically the effect of a spatially uniform change in wettability in the range of intermediate contact angles expected for the GDLs, i.e. typically in the "critical" range [70–115°], in model two-dimensional systems. However, a three-dimensional version of this model is not available and direct simulations at the pore scale based on lattice Boltzmann methods, e.g. [14], or Navier–Stokes equations are too much computational time consuming for a convenient exploration of the effect of the contact angle. Thus, the most convenient way at the moment for exploring a change in wettability within the framework of three-dimensional PNM is to vary the fraction of hydrophilic pores.

The paper is organized as follows. The pore network model is presented in Section 2. In Section 3, we discuss in more depth the wettability of GDL from comparisons between pore-network simulations and measured capillary pressure curves. The computation of the effective diffusion coefficient and of the relative permeabilities, two important parameters for the continuum models, is presented in Section 4. Then, we present in Section 5 simulations of the water invasion of a GDL considering various wettability scenarios so as to explore the influence of wettability on pore blockage by the water. Note that the structural changes (pore sizes, porosity, etc.) that might result from varying the load in PTFE are not considered.

2. Pore network model (PNM)

The PNMs are based on the representation of the pore space in terms of a network of pores (or sites) connected by throats (or bonds). The "pores" roughly correspond to the larger voids whereas the throats connecting the pores correspond to the constrictions of the pore space. In the most advanced developments,

see for example [15] and references therein, the pore network is constructed from direct imaging, usually by micro-X-ray computerized tomography. An alternative is to use synthetic 3D structure generated numerically. This leads to "morphological" pore networks since the pore network is constructed directly from the "real" microstructure. The method is for example illustrated in [3] with a two-dimensional network constructed from a model fibrous medium. Although using morphological pore networks is certainly the most attractive approach, using simpler pore networks can be very instructive. In fact, morphological pore networks have rarely been used in relation with fuel cell related problems, see however [16]. Most of the studies, e.g. [3,17–21], are based on simpler networks, such as cubic networks in 3D or square networks in 2D. Computations are easier than for a morphological network and it is still possible to incorporate information from the "real" microstructure such as throat size and pore size distributions. Also, to understand some effects, a simple network is generally sufficient. Accordingly with the above, a simple cubic network is considered in what follows. As discussed in several places in the paper from comparisons with experimental data, this simple model seems to be not always sufficient, however, to represent fibrous materials accurately. The development of advanced pore network models for fibrous materials is in fact an open area of research. We believe, however, that the model considered in the present study is sufficient to explore the effect of a mixed wettability, which is the primary objective of the study.

As sketched in Fig. 1, pores of cubic shape are regularly placed on a 3D cartesian grid (with a denoting the lattice spacing, that is the distance between two adjacent pores). Two first neighbour pores are linked by a channel of square cross-section. Such a channel is referred to as a bond or throat. The pore size d_p, which corresponds to the diameter of the largest sphere inscribed within the pore, is randomly distributed according to a probability law in the range $[d_{p\min}, d_{p\max}]$. As in [17], a Weibull distribution is used in the present study. More precisely, the pore sizes are randomly specified using the expression $d_p = d_{p\min} + (d_{p\max} - d_{p\min}) \left\lfloor \{-\delta \ln(\lambda(1 - \exp(-1./\delta)) + \exp(-1./\delta))\}^{1/\gamma} \right\rfloor$ with $\delta = 0.1$, $\gamma = 4.7$; λ is the random number drawn in the interval [0,1]. The size d_t of a throat is then specified as equal to the minimum size of its two adjacent pores, $d_t = \min(d_{pi}, d_{pj})$. Simulations presented in what follows have been performed with $a = 25.2\ \mu m$, $d_{p\max} = 25\ \mu m$, $d_{p\min} = 10\ \mu m$. These values are representative of pore size distributions in GDL, e.g. [17], and lead to an average porosity ε of 0.77 for our model porous medium.

The network size is characterized by the number of pores placed in each direction. We consider a $40 \times 40 \times 10$ network. As discussed in [21], this size is considered as representative of a GDL unit cell with the in-plane extension (~ 1 mm) corresponding roughly to the distance between two channels of the bipolar plate. The pore network is fully hydrophobic (resp. hydrophilic) when all throats and pores are hydrophobic (resp. hydrophilic). In a mixed wettability pore network a fraction f of the pores and of the throat are randomly specified as hydrophilic ($\theta \sim 80°$). The remaining pores and throats are hydrophobic ($\theta \sim 115°$). There are therefore a fraction $1 − f$ of hydrophobic pores and throats in the network. For convenience, such a network will be referred to as a network containing a fraction f of hydrophilic "pores" but this means in fact that the fraction of hydrophilic throats and the fraction of hydrophilic pores are both equal to f. No correlation is introduced between the wettability of a pore and that of adjacent throats. A realization of network is obtained by assigning pore and throat size randomly and θ (80° or 110°) randomly for a given hydrophilic fraction. All the results presented in the following are averaged over 100 realizations (the results presented in [22] indicate that this is a sufficient number of realizations to obtain the average behaviours).
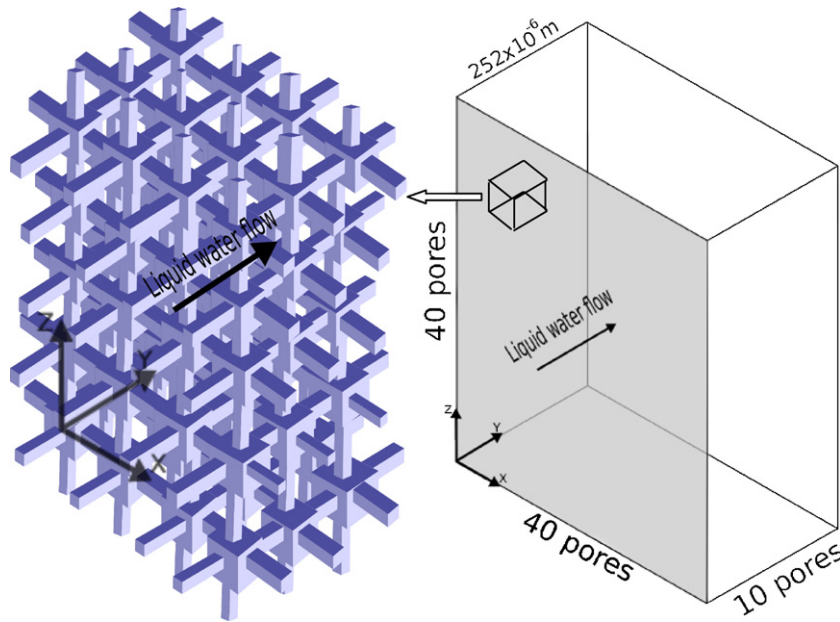
Fig. 1. Schematic of cubic pore network. The size of network is $40 \times 40 \times 10$. As shown in the figure, the GDL thickness is 252 μm and there are 10 pores 25.2 μm apart across the GDL.

3. Local invasion rules

It is widely admitted that liquid invasion in a GDL can be computed in the quasi-static limit, that is the invasion is controlled by capillary effects, see [3] or [22] for more details. When the computation of properties is performed in relation with continuum models, the classical assumption of local capillary equilibrium is assumed and this corresponds again to quasi-static water distribution in the pore space. Accordingly, the influence of viscous effect is ignored in this paper and only capillary effects are taken into account. When the porous matrix is sufficiently hydrophobic, quasi-static water invasion can be simulated rather simply using the well-known invasion percolation (IP) algorithm [23]. When the medium is hydrophilic, the computation is significantly more involved because of cooperative mechanisms controlling the growth of the interface between the two fluids within the pore space [3,21], and references therein. A relatively simple but approximate algorithm was, however, proposed in [24], see also [25]. A similar algorithm is used in the present study. Note that this algorithm becomes identical to the IP algorithm when the network is fully hydrophobic ($f = 0$). Hence all the simulations are performed using the local expressions given in this section. The capillary pressure is conventionally defined as

$$p_c = p_w - p_g \tag{1}$$

i.e. as the difference between the pressure in the water and the pressure in the gas phase. Then we define the capillary pressure threshold p_{cth} associated with each element, pore or throat, of the pore network. The capillary pressure threshold of a throat is expressed using the Young–Laplace equation as

$$p_{cth} = -\frac{2\sigma \, \cos\theta}{r_t} + P_1 \tag{2}$$

where $r_t \approx d_t/2$; P_1 is a numerical constant with $P_1 = 0$ for $\theta = 115°$ and $P_1 = 5500$ for $\theta = 80°$. The motivation for the introduction of constant P_1 is given in the next section (Section 4). Eq. (2) is only an approximation. One can refer for example to [26] for a more accurate evaluation of the capillary pressure threshold of a throat of square cross-section. Eq. (2) leads to the correct hierarchy in terms of capillary pressure threshold and this is sufficient for the

pore network simulations (PNS). The contact angle θ is measured in the denser fluid (water); σ is the surface tension. The capillary pressure threshold of a pore depends on the number n of adjacent throats filled with the less dense fluid (gas phase) and reads

$$p_{cthp} = -\frac{2\sigma \, \cos\theta}{r_n} + P_1 \tag{3}$$

where

$$r_n = \frac{d_p}{2} + \sum_{i=1}^{n} b_i x_i r_{ti} \tag{4}$$

where d_p is the pore size, r_{ti} is the half-size of a adjacent throat filled with air, x_i is a random number drawn in the range 0–1. The coefficients b_i are defined as: $b_1 = 0.$, $b_2 = 5./\bar{r}_t$, $b_3 = 10./\bar{r}_t$, $b_4 = 50./\bar{r}_t$, $b_5 = 100./\bar{r}_t$; $\bar{r}_t$ is the mean throat radius (mean of the pore surrounding throat radii). When n is small, many surrounding throats are already filled with water and water invasion of the pore is favoured (when $\theta < 90°$). As discussed in [27], Eqs. (2)–(4) define invasion potentials. The element, pore or throat, of lowest potential (=lowest capillary pressure threshold) is invaded at each step of invasion to simulate a quasi-static invasion (see Section 7). The coefficients b_i are specified so as to obtain a compact pattern in a 100% hydrophilic pore network. The values of these coefficients indicated above lead to the desired pattern. One can refer to the Appendix in [27] for more details on the invasion potential hierarchy needed to simulate adequately the quasi-static invasion of a porous medium by a wetting fluid.

As explained in the next section, the constant P_1 is added to Eqs. (2) and (3) to generate positive capillary pressures in fully or partially hydrophilic networks so as to be in agreement with available experimental data. This might appear as quite artificial. However, it should be realized again that the key point is that Eqs. (2)–(4) lead to a correct hierarchy in terms of local invasion capillary thresholds, i.e. for example a hydrophilic element is always preferentially invaded compared to a hydrophobic one. Adding the constant P_1 does not affect this hierarchy and therefore the simulated water distributions and consequently the results presented in what follows, except as regards the capillary pressure curve for which a much better agreement is obtained by introducing the constant P_1.
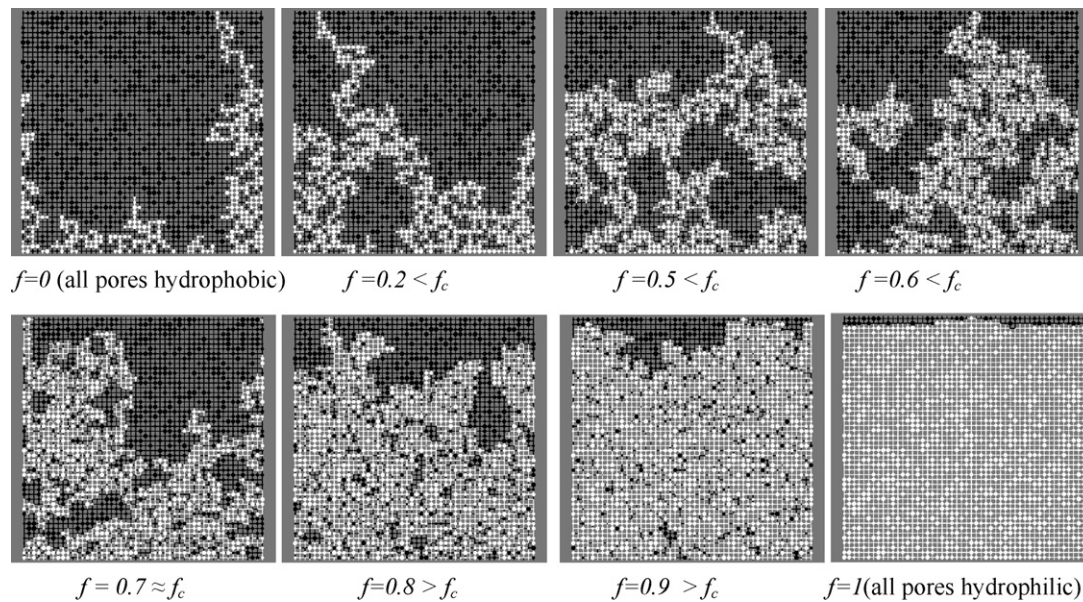
Fig. 2. Invasion patterns for various values of the hydrophilic pore-throat fraction f in a 2D 50×50 square network. The invading fluid (water in white) is injected from the bottom using the algorithm described in Section 7. The defending fluid (in black) escapes from the top. A capillary fingering pattern is observed for $f \sim 0$. A compact pattern is obtained for $f \sim 1$. The pattern obtained for $f \sim f_c$ resembles the capillary fingering pattern but actually results from the fact the percolating subnetwork formed by the hydrophilic pores and throats is a percolation cluster. An invasion percolation cluster ($f \sim 0$) is about the same fractal object as the hydrophilic pores percolation cluster ($f \sim f_c$). This is why both cases ($f \sim 0$ and $f \sim f_c$) lead to the same type of phase distribution despite the change in the local mechanisms controlling the growth of the liquid/gas interface in the hydrophobic regions and the hydrophilic ones respectively. For this bond-site percolation network, f_c is approximately equal to 0.7.

The two-dimensional invasion patterns obtained at breakthrough using these local rules in a square network, see Section 7 for the details on the invasion algorithm, and shown in Fig. 2, exemplify the effect of the change in wettability. As can be seen, the patterns are roughly similar (i.e. ramified and not compact) as long as f is lower than the so-called percolation threshold f_c. As discussed in more details in Section 7, f_c is the critical value above which at least one continuous path of hydrophilic pores and throats exists between the inlet and the outlet. The pattern becomes more and more compact as f increases above f_c. In a hydrophilic network ($f = 1$), the pattern is characterized by an almost flat travelling front. We chose to present two-dimensional patterns in Fig. 2 only for clarity since a 2D pattern is much easier to represent than a 3D pattern. Analogous patterns are obtained in 3D as well and this should be kept in mind when discussing the results presented in the next sections. All the results presented in the remaining of the paper are for a 3D $40 \times 40 \times 10$ network.

4. Capillary pressure curve

The capillary pressure curve $P_c(S)$ (or equivalently $P_c(S_g)$ where $S_g = 1 - S$, where S is the saturation of the denser phase (=liquid water) and S_g is the saturation of the gas phase) is one of the key input parameters for the traditional continuum models. Also, the capillary pressure curve gives information about the overall wettability of a porous system, e.g. [1,5]. As exemplified for example in [6], pore network models can be used to determine $P_c(S)$. The capillary curve is computed using an algorithm similar to the one presented in [22], but which now takes into account the presence of hydrophilic pores. This algorithm is supposed to mimic the experimental procedure used for example in [1]. Due to the random fluctuations, $P_c(S)$ has to be determined over many realizations of the network. For a given realization, we start with a dry network and determine the overall capillary pressure as a function of S for successive states of hydrostatic equilibrium corresponding to small increment dP_w in the liquid water pressure (the gaseous

phase pressure is kept constant). The algorithm used to determine the saturation evolution right after a pressure increment reads:

1. Identification of each element (pore or throat) that can be invaded, that is each element occupied by the gaseous phase such that its capillary pressure threshold p_{cth} is lower than the imposed pressure difference $P_w - P_g$ between the two fluids.
2. Identification of clusters formed by the elements identified in (1) using a cluster identification algorithm.
3. Identification of clusters among the clusters identified in (2) in contact with the invading phase.
4. Invasion of all clusters identified in (3).
5. Computation of overall saturation.

Using this algorithm leads to the results shown in Fig. 3. The results are compared with the experimental results presented in [1] in Fig. 3a. As can be seen, there is a good agreement between the simulations and the experimental results over a wide range of intermediate saturations for both the fully hydrophobic and the fully hydrophilic network. There are clearly discrepancies for the low and high saturations. We have changed the pore size distribution (PSD) using a uniform distribution (each pore size has the same probability) and observed that a slightly better agreement could be obtained. Thus this suggests that these differences could be explained in part by the choice of the PSD. For example, the capillary pressure level reached in the experiments ($\sim$14 kPa) is much higher than in the simulations. This is probably due to the fact that very small pores are not considered in the simulations. If we make the fair assumption that the experimental results are fully reliable, the comparison shown in Fig. 3a could be an indication that the problem comes also from the pore network model. A simple cubic pore network as considered here is perhaps not sufficient to simulate accurately the capillary pressure curve and more refined pore network models, i.e. typically morphological or topological pore network models as mentioned in the introduction, would deserve to be developed. As mentioned before, this is however an open area of research as regards fibrous materials and therefore this is
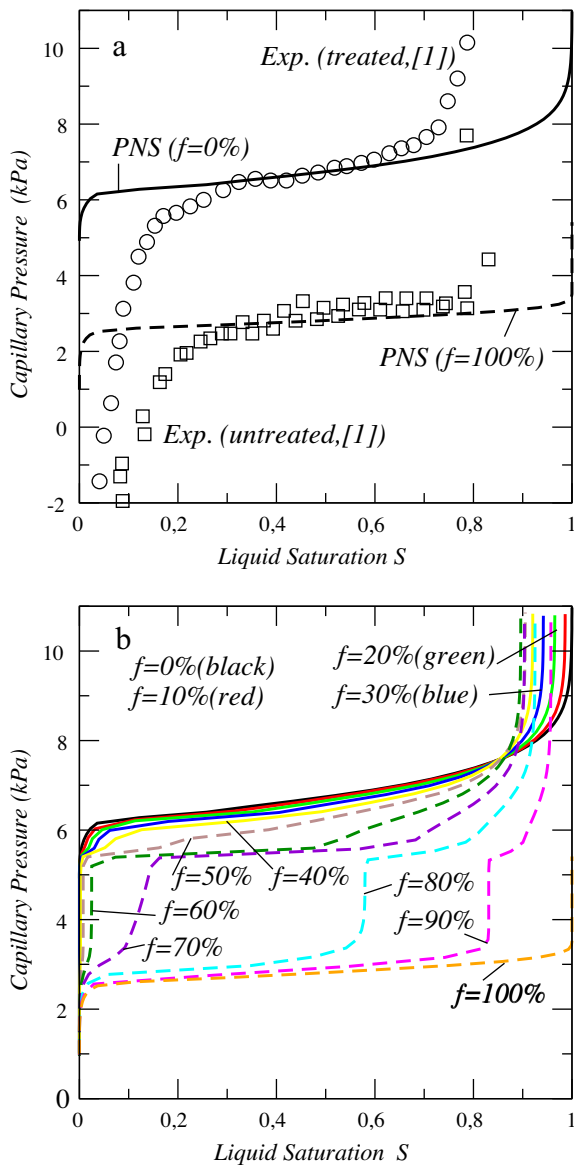
Fig. 3. Computed water invasion capillary pressure curve for various fractions of hydrophilic pores (solid line for a hydrophilic pore fraction below the percolation threshold f_c, dashed line above f_c): (a) comparison with experimental data: the empty circles and squares correspond to the measured capillary pressure curves for PTFE treated Toray TGPH-090 (empty circles) and untreated Toray TGPH-090 (empty squares) (imported and adapted from [1]). The computations were performed with a contact angle of 115° in the hydrophobic pores and of 80° in the hydrophilic pores; (b) influence of the fraction of hydrophilic pores f on the computed capillary pressure curve.

a hydrophilic medium. It is however well known that the capillary pressure threshold of a constriction depends not only on the contact angle but also on the constriction geometry, e.g. [28]. The consideration of a more realistic geometry, e.g. [3,28], leads to positive capillary pressure threshold. To mimic this effect, we have chosen the simpler approach consisting to add a positive constant P_1 in Eqs. (2) and (3) for the contact angle $\theta = 80°$. As can be seen from Fig. 3a, a reasonable agreement with the experimental data is obtained with $P_1 = 5500$ in Eqs. (2) and (3). The model being adjusted on available capillary pressure experimental data, we now discuss the effect of mixed wettability on the capillary pressure curve.

As can be seen from Fig. 3b, the results for a fraction of hydrophilic pores lower than about 50% are practically identical to those for a fully hydrophobic network except for the high saturations. In passing, we note that the behaviour for the high saturations is closer to the experimental results (Fig. 3a treated GDL) when $f = 40\%$ for example. It is therefore tempting to conclude that this is an indication that the treated GDL is in fact partially hydrophobic but again more advanced pore network models are needed to confirm this from PNS. Interestingly, the influence of Teflon loading on the (water invasion) capillary curve is found to be quite weak in the experiments for all the loading tested (up to 40 wt%), e.g. [1]. A similar result is found numerically provided that the fraction of hydrophilic pores is lower than about 50%, which roughly corresponds to the hydrophilic pore/throat network percolation threshold discussed in Section 7. When the fraction of hydrophilic pores is greater than 50% the results are markedly different as can be seen from Fig. 3.

In summary, the comparison between the $40 \times 40 \times 10$ pore network simulations and the experimental results presented in this section shows (i) that the pore network model can simulate reasonably well the capillary pressure in a fully hydrophobic or a fully hydrophilic system, (ii) that the assumption of mixed wettability is consistent with the available data on the GDL capillary pressure curve when the fraction of hydrophilic pores is lower than about 50% and (iii) that more refined pore network models are needed for obtaining a still better match with the experimental data. Our simulations also show that it cannot be readily concluded from the measurement of the water invasion capillary pressure curve that the system under study is fully hydrophobic (as suggested in [1] from the ToF-SIMS data) since the curve is not sensitive, except however in the range of the high saturations, to a change in the fraction of hydrophilic pores up to relatively high fractions of hydrophilic pores ($f \leq 50\%$).

5. Relative permeabilities

The relative permeabilities are also important parameters of continuum models. In this section we discuss the influence of the fraction of hydrophilic pores on the relative permeabilities. The procedure for computing the intrinsic permeability and the relative permeabilities is described in several papers, e.g. [22] and references therein, and therefore is only briefly summarized here. Local hydraulic conductances are assigned to each throat and pore. The same expressions as the ones considered in [17] are used. Expressing the mass conservation equation at each pore yields a linear system of equations that is solved numerically and gives the pressure at each node (pores) of the network. As boundary conditions, arbitrary pressures P_{outlet} and P_{inlet} are prescribed at inlet and outlet surfaces of network with $P_{inlet} > P_{outlet}$. This yields the total flow Q over the network. Once Q is determined, the permeability K of the network is found from Darcy's law. For determining the relative permeabilities (K_r), we combine the procedure described in Section 4 to determine the fluids distribution within the network and the computation of permeability described above. For example the
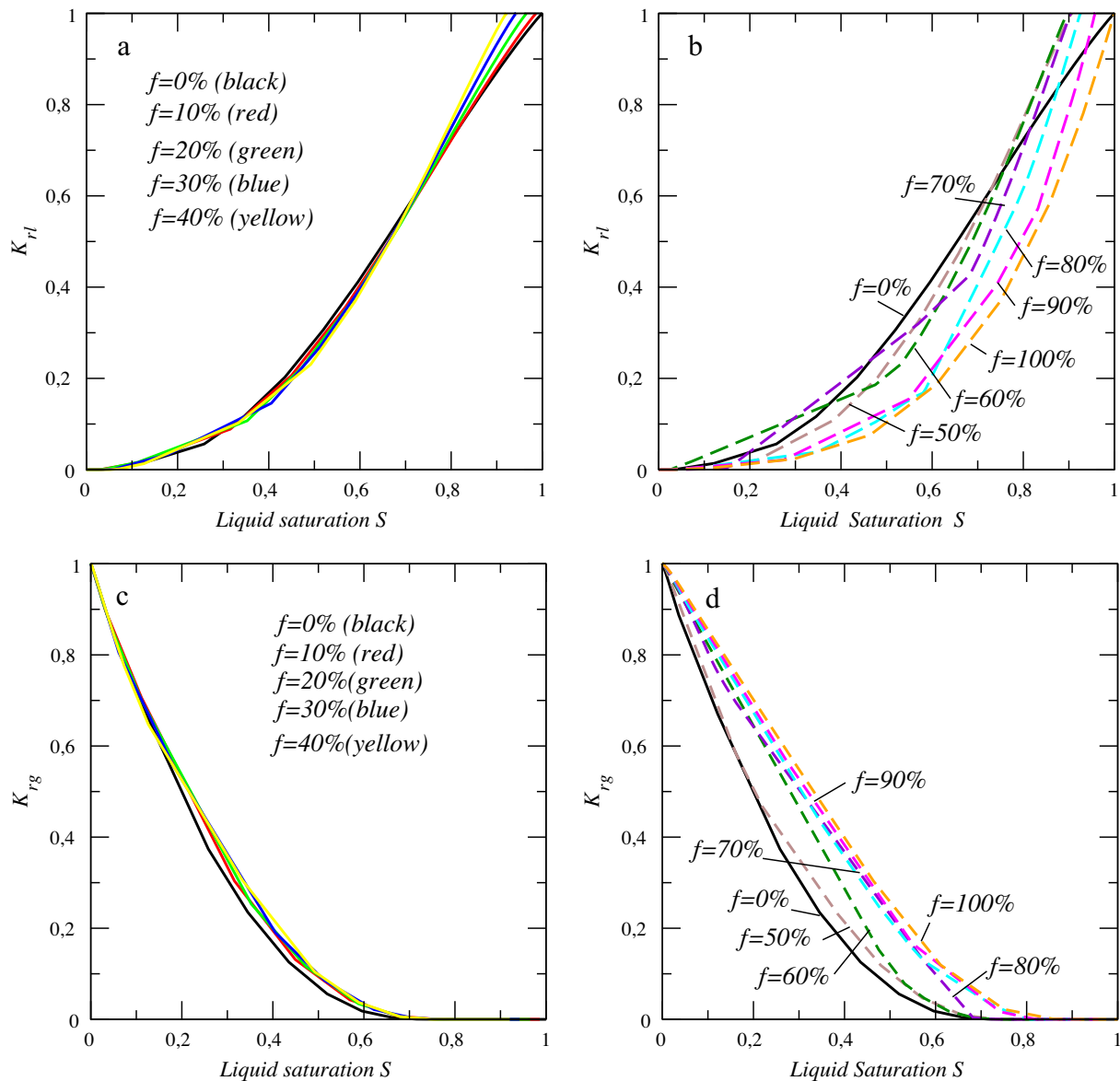
left for a future work. Here we consider that the good agreement obtained over a wide range of intermediate saturations is sufficient to explore with confidence the effect of a mixed wettability with the present model.

Another aspect of the experimental results deserves to be pointed out. Except for the low saturations below 0.1, the experiments lead to a positive capillary pressure (the pressure in the liquid water is greater than in the gas phase) for both the treated and untreated GDLs. This was expected for a treated GDL since the contact angle on PTFE is significantly greater than 90°. For the untreated GDL, the contact angle is expected to be lower than 90° ($\theta \sim 80°$) and the naïve consideration of the fibrous materials as a bundle of straight tubes leads immediately to the conclusion that the capillary pressure should be negative (with our convention) in

Fig. 4. Through-plane relative permeability of liquid water (a, b) and gas (c, d) as a function of liquid saturation for various fractions of hydrophilic pores (solid line for a hydrophilic pore fraction below the percolation threshold f_c, dashed line above f_c).

effective permeability $K K_{rg}$ of the gas phase is determined using the same procedure as for the intrinsic permeability except that only the sub-network occupied by this phase is considered. Again more details on this type of computation can be found in [17].

The evolutions of K_r for our network are shown in Fig. 4 for various fractions of hydrophilic pores and correspond to the through-plane relative permeability. As can be seen from Fig. 4, the relative permeability curves are not very sensitive to the fraction of hydrophilic pores in the range of f [0–50%]. For a given intermediate value of the saturation ($S \sim 0.5$ for example), the gaseous phase relative permeability increases slightly with the fraction of hydrophilic pores whereas the opposite behaviour is observed for the liquid water relative permeability. As can be seen from Fig. 4b and d, the sensitivity of the relative permeabilities to the hydrophilic pore fraction is much more marked for $f > 50\%$. For again an intermediate value of the saturation, $S \sim 0.4$–0.5, the gas (resp. liquid) relative permeability is significantly greater (resp. lower) in the hydrophilic network ($f = 100\%$ in Fig. 4). As discussed in the next Section, Section 6 below, this can be explained by the size of the throats selected

during the invasion of the network by the liquid. Narrower throats are favoured in a hydrophilic network whereas the invasion occurs preferentially in wider throats in a hydrophobic network.

Experimental measurements of relative permeabilities are reported in [29] for a GDL treated with a 5 wt% PTFE solution and in [30], but only for untreated (non-teflonized) materials. Our simulated values of the gas phase relative permeability are somewhat greater than the experimental data reported in [29] but in reasonable agreement with the lattice Boltzmann computation of K_{rg} also reported in [29]. More accurate experimental data would be necessary to make a more informative comparison. Our results for a sufficiently hydrophobic network are also in good agreement with the lattice Boltzmann computation of K_{rg} and K_{rl} reported in [14] for a small volume of a model hydrophobic GDL.

The measured values of through-plane gas phase relative permeability reported in [30] are found to be very low, much lower than predicted with the PNM or reported in [14,29]. According to [30] this low values are attributed to an experimental artefact. However, the GDLs being untreated in this experiment, compact

invasion patterns are possible, see Fig. 2 and Ref. [3], and might also explain in part the results reported in [30].

6. Effective binary diffusion coefficient

The (through-plane) effective binary diffusion coefficient D_{eff} is an interesting parameter because it reflects the effect of the pore blockage by the water on the gas transport through the GDL. In fuel cell modelling literature, $D_{eff}(S)$ is often represented by expression of the form, e.g. [17]

$$D_{eff}(S) = \varepsilon^{1.5}(1-S)^{1.5}D \tag{5}$$

where D is the binary molecular diffusion coefficient. Here we use the pore network model to compute D_{eff} and it is shown that Eq. (5) does not lead to a good match with the pore network simulations.

The procedure for computing the effective binary diffusion coefficient from pore network simulations is analogous to the one for the effective permeability and is described for example in [17]. For each stage of pore network occupancy by the water obtained as described in Section 4, local diffusive conductances are assigned to each pore and throat occupied by the gas phase and a linear system of equations is formed by expressing the mass conservation at each gaseous pore of the network and imposing a concentration difference across the network. Solving numerically the linear system give the concentration of the considered species (i.e. oxygen) at each gaseous pore of network. This allows to compute the diffusive flux across the network and then to determine the effective diffusion coefficient from the mathematical expression of the through-plane macroscopic flux J, which is expressed as

$$J = AD_{eff}\left(\frac{C_{inlet} - C_{outlet}}{L}\right) \tag{6}$$

where A the cross-section area of the porous medium, L is the porous medium thickness and C_{inlet} (resp. C_{outlet}) is the concentration imposed at the inlet (resp. outlet). The procedure used here is exactly the same as the one described in [17] and therefore the details are not given again for the sake of brevity.

The simulation results are presented in Fig. 5. They are not surprisingly in good agreement with the PNM simulations presented in [17] for a fully hydrophobic network since the computational procedure is the same as in [17] (for the case referred to as "case 1" in [17]). More interesting is the impact of the fraction of hydrophilic pores f. For a given intermediate saturation, D_{eff} increases significantly with f for $f > f_c$, i.e. $f > 50\%$ in Fig. 5. Thus a rapid conclusion would be that a sufficiently hydrophilic GDL is better since the effective diffusion coefficient increases with f for $f > f_c$. However, one should keep in mind that the phase distribution evolution is obtained here as described in Section 4, i.e. as the result of successive states of hydrostatic equilibrium corresponding to small increment in the pressure of the water dP_w. This procedure leads to the preferential invasion of the smallest throats and pores in a hydrophilic network and to the preferential invasion of largest pores in a hydrophobic networks (this can be easily seen from the expressions of capillary pressure thresholds in Section 3). Therefore, for a given saturation, the fraction of the pore space left free for the gas transport is primarily made of large pores and throats in a hydrophilic network and of small pores and throats in a hydrophobic network. This explains why the effective diffusion coefficient is greater in the hydrophilic network and increases with f for $f > f_c$. The same explanation holds as regards the evolution of the relative permeabilities reported in Section 5.

As presented in the next sections, the conclusion is exactly the contrary, i.e. a too hydrophilic GDL is detrimental to gas transport, when water invades the GDL according to the invasion rules described in Section 7. As explained in Section 4, the procedure used in Sections 4–6 to compute the invasion of the network by the liquid
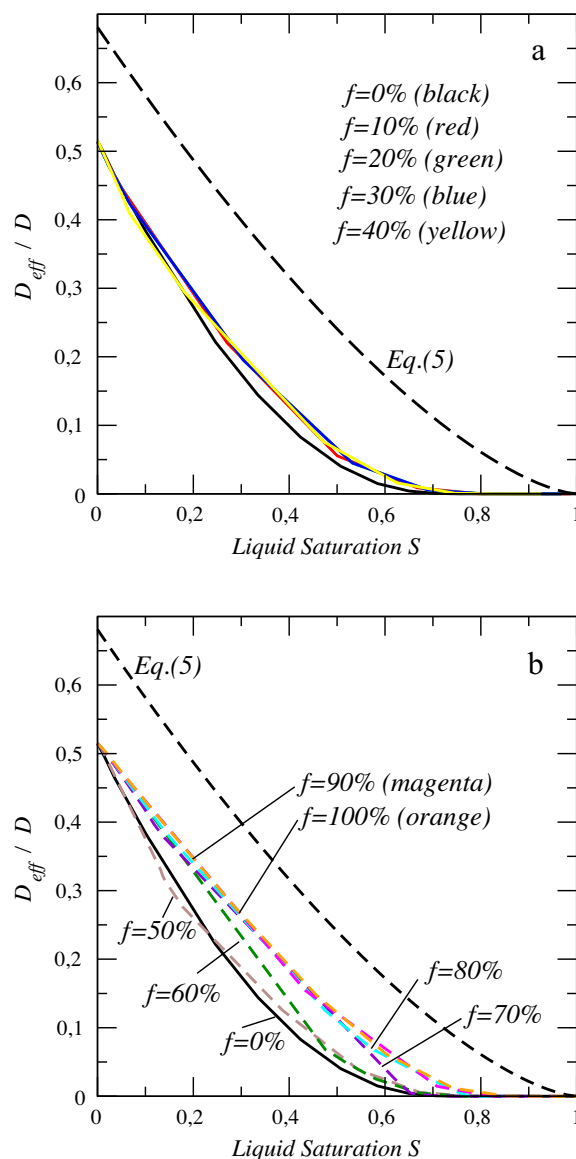

Fig. 5. Evolution of through-plane binary effective diffusion coefficient as a function of liquid saturation for various fractions of hydrophilic pores (solid line for a hydrophilic pore fraction below the percolation threshold f_c, dashed line above f_c): (a) fractions of hydrophilic pores below the percolation threshold, (b) fractions of hydrophilic pores above the percolation threshold.

water corresponds to the typical procedure used to measure a capillary pressure curve. In this case, the water invasion is controlled by increasing step by step the pressure difference between the two fluids. The completely different invasion condition used in the next sections corresponds to imposing a small invasion flow rate. This condition is supposedly much more representative of water invasion in a GDL in a fuel cell than the pressure difference controlled invasion. This illustrates that care should be exercised when analyzing two-phase flows in this type of system or when devising ex situ experiments for characterizing GDL transport properties.

As can be seen from Fig. 5, Eq. (5) overpredicts $D_{eff}(S)$ significantly. Thus using Eq. (5) leads to underestimating the mass transport limitation in the gas diffusion layer. The comparisons with the experimental results reported in [31] (for a dry GDL) indicate that this holds for all the existing effective diffusion theoretical models. Compared to the experimental results presented in [31] ($D_{eff}(0)/D \sim 0.32$ for an untreated GDL), the PNM also overpredicts D_{eff} with $D_{eff}(0)/D \sim 0.5$, but less than the available theoretical

models ($D_{eff}(0)/D \sim 0.6$–0.7, see [31]). Although the experimental evaluation of D_{eff} is not easy due to the thin nature of a GDL and therefore additional measurements are desirable, this can be again an indication that better pore network models of fibrous materials need to be developed. In passing, we note that the experimental results reported in [31] indicate a significant influence of Teflon treatment on $D_{eff}(0)$. This would indicate that the Teflon treatment modifies the pore space sufficiently for affecting the effective diffusion coefficient but not, according to [1], for affecting the capillary pressure curve. This is somewhat surprising and would need further clarification. As mentioned before, this effect of Teflon on pore size and pore volume is not taken into account in our simulations.

7. Quasi-static invasion

In the preceding sections, the PNM was essentially used to compute some parameters of the classical phenomenological model of two-phase flow in porous media. This is a somewhat obvious objective since most of the simulations of two-phase flow in fuel cells are based on this classical model. As discussed for example in [22], there are, however, serious concerns about using the classical phenomenological model to simulate water invasion in a thin system like a GDL. There is a lack of length separation (a GDL is typically a few pore sizes thick) and the dominant two phase flow regime in a hydrophobic GDL is expected to be the capillary fingering regime, a regime which leads to fractal distributions of the fluids within the pore space and which is therefore not compatible with the traditional concept of R.E.V. (representative elementary volume) underlying the classical continuum approach. As a result, the classical continuum model is likely to lead to poor approximations of the real fields and this is illustrated in [22]. Because of the weaknesses of the classical model, it can be much more instructive to use the PNM for predicting directly the water invasion pattern within the GDL.

As mentioned before, water invasion in a GDL for the operating conditions of a PEMFC is expected to be dominated by capillary effects and therefore can be simulated as a quasi-static invasion process. As briefly evoked in the preceding section, Section 6, one can distinguish two main types of boundary condition (B.C.) to simulate a quasi-static liquid water invasion: (i) pressure B.C. and (ii) flow rate B.C. As described in Section 4, the pressure B.C. consists in increasing step by step the pressure difference between liquid water and the gas phase. The flow rate B.C. consists in assuming that liquid water invades the system as a result of a small imposed flow rate at the inlet. In this case, it is classically assumed that all the throats at the inlet of the network are connected to a continuous liquid reservoir at the inlet and that liquid is very slowly injected at a specified flow rate in this reservoir. This increases very gently the pressure (supposed uniform) in the reservoir until the invasion of the adjacent porous medium can start. Then the pressure in the reservoir typically fluctuates around a mean value as the water invasion continues in the porous medium up to breakthrough. Starting from a dry network, the corresponding invasion algorithm reads,

(1) Identify the element (pore or throat) adjacent to the already invaded region that has the lowest invasion capillary pressure threshold (see Section 3).
(2) Invade the identified element in 1 and update the phase distribution in the network. Return to (1).

The invasion stops when water reaches the GDL outlet. This stage of the invasion is referred to as the breakthrough (BT).

As discussed in [22] or [32], there is still, however, a question about the flow rate boundary condition to impose at the inlet of the
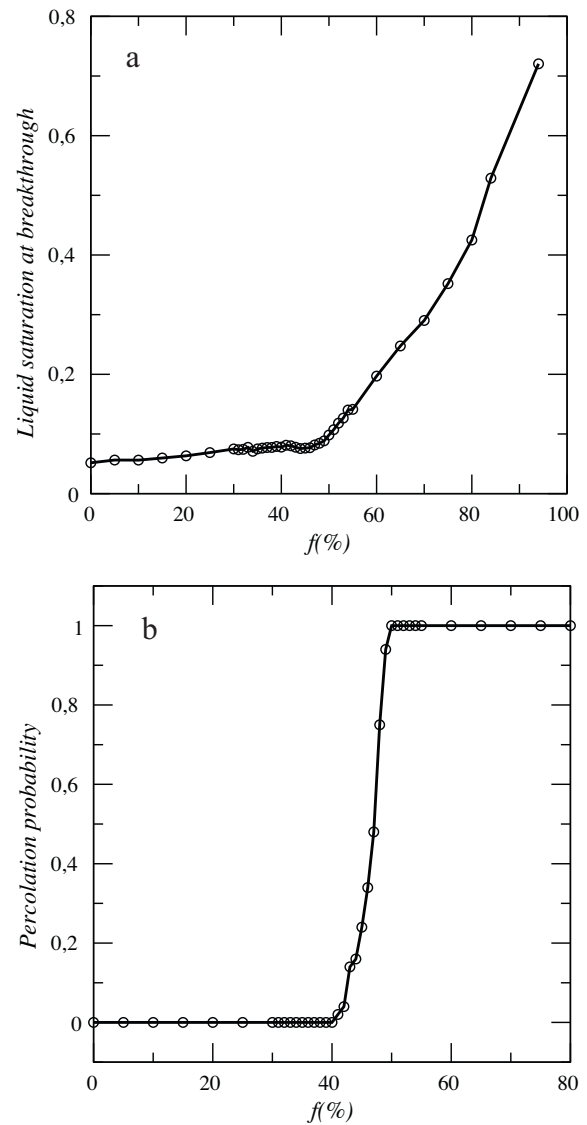

Fig. 6. (a) Evolution of overall liquid saturation at breakthrough as a function of the fraction of hydrophilic pores; (b) percolation probability as a function of the fraction of hydrophilic pores.

GDL. As discussed above, the classical flow rate boundary condition is to assume that all throats of the network at the inlet are connected to a water reservoir. This condition can be representative of flow rate controlled ex situ experiments, e.g. [33]. For a GDL in a fuel cell, the boundary condition can be expected to be different since water comes not from a reservoir but from adjacent porous layers (MPL and catalyst layer). As discussed in [32], it is envisioned that water enters rather the GDL through a series of independent injection points. As shown in [32], the boundary condition has a significant impact on the GDL water occupancy. Thus it would be interesting to consider the multiple injection points boundary condition as well. For the sake of brevity, we only consider, however, the reservoir type boundary condition. The effect of the multiple injection points boundary condition will be explored in a future work.

The evolution of the overall liquid water saturation S at BT as a function of the fraction of hydrophilic pores f is shown in Fig. 6a. As in any classical percolation problem [34], the hydrophilic pores and throats form isolated hydrophilic pore and throat clusters for sufficiently low values of f. When f is sufficiently large, there exists a cluster of hydrophilic pores and throats spanning the system. The critical hydrophilic pore fraction below which such a cluster does
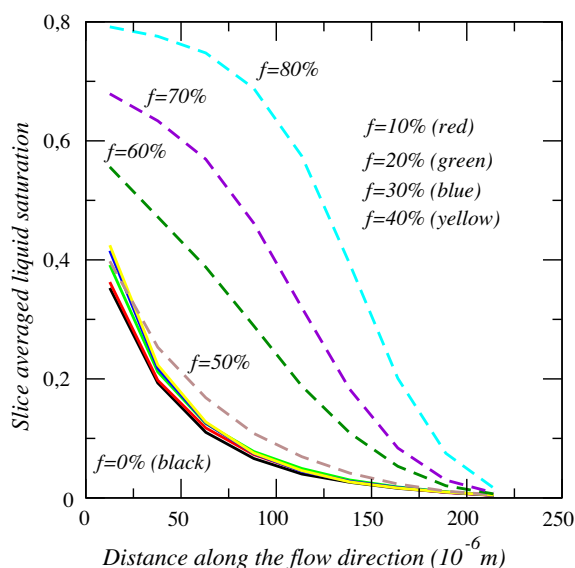
Fig. 7. Liquid saturation profile along the thickness at breakthrough for various fractions of hydrophilic pores (solid line for a hydrophilic pore fraction below the percolation threshold f_c, dashed line above f_c).

Fig. 8. Evolution of through-plane binary effective diffusion coefficient at breakthrough as a function of the fraction of hydrophilic pores.

not exist is the percolation threshold f_c. In a finite size system, the percolation transition is not sharp and some realizations are percolating below f_c whereas others are percolating for values of f greater than f_c. This is illustrated in Fig. 6b, which shows the evolution of the percolation probability F as a function of f (for a given value f, F is the fraction of percolating realizations among the 100 generated realizations). The percolation threshold corresponds to the rapid transition in the evolution of F in Fig. 6b. As can be seen from Fig. 6b, f_c is of the order of 46–48% for our system.

Since liquid water favours hydrophilic elements, liquid water invasion takes place through a path of hydrophilic pores and throats above f_c and the hydrophobic pores and throats are left free of water, i.e. available for gas transport. Below f_c, some hydrophobic pores and throats are necessarily invaded since the hydrophilic pores and throats do not form a percolating cluster. However, a hydrophilic cluster is systematically fully invaded when liquid water meets such a hydrophilic cluster during the invasion. We know from Section 3 and Ref. [3] that the invasion pattern and the local invasion mechanisms are significantly different for $\theta \approx 80°$ and $\theta \approx 110°$ (as illustrated also in Fig. 2). Interestingly, this does not have, however, a great impact on the overall saturation at breakthrough over a large range of f, i.e. as long as $f \leq f_c$ as shown in Fig. 6a. This can be qualitatively understood as follows. For f close to 0, the water invasion process is essentially an invasion percolation (IP) process as discussed in Section 3. As it is well known, the subset of pores invaded at breakthrough as a result of the IP process is very similar to an ordinary percolation cluster, i.e. the percolating cluster formed by the hydrophilic pores and throats at f_c. Hence, since the pore size distribution is generally narrow in a GDL, we expect that $S(0) \approx S(f_c)$. For intermediate f between 0 and f_c, the invaded pore subset can be envisioned as a chain of invaded hydrophilic pore clusters connected by paths of hydrophobic pores, i.e. a structure close to a percolation cluster at f_c. The saturation increases rapidly above f_c. The minimum saturation in Fig. 6a is observed for a fully hydrophobic network ($f = 0$). Interestingly, a local minimum saturation is observed in Fig. 6a for $f \approx f_c$. The reasons for the existence of this local minimum are, however, unclear and this is left for a future work.

The main practical conclusion from the results shown in Fig. 6, is that the PTFE load (assuming here that there is a direct link between the PTFE load and the fraction of hydrophobic pores) has
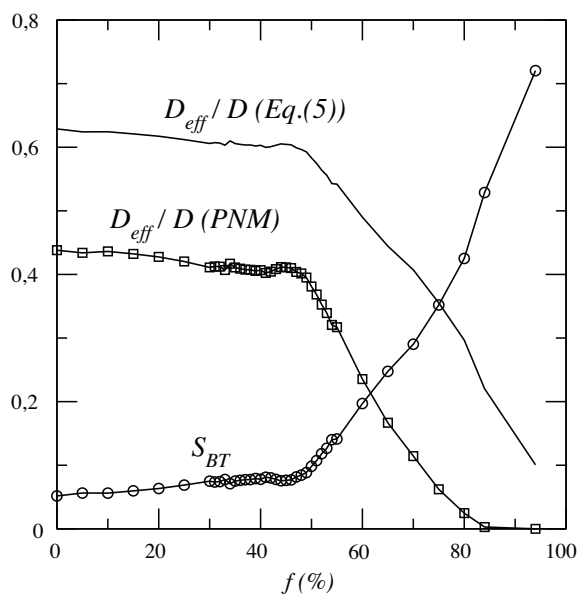
little impact on the water management problem as long as the fraction of hydrophilic pores and throats is not significantly larger than the percolation threshold of the system.

This is further illustrated with the saturation profiles at BT depicted in Fig. 7. These profiles are obtained by computing the saturation over successive slices of network in the through-plane direction (10 slices for our $40 \times 40 \times 10$ network) for each realization. Again the profile is not very sensitive to the fraction of hydrophilic pores as long as $f \leq f_c$ except near the inlet where the minimum saturation in the first slice ($S \sim 0.35$) is obtained for a fully hydrophobic network whereas $S \sim 0.43$ for f approaching f_c (curve for $f = 40\%$ in Fig. 7). As can be seen from Fig. 7, the pore blockage by the water at BT increases significantly for $f > f_c$. Again, these results suggest that a loss in hydrophobicity in our model system (assuming for instance a fully hydrophobic network initially) should not lead to a discernable decrease in the fuel cell performance in a first phase (i.e. as long as f increases below f_c) and then to a significant loss in performance when the GDL becomes sufficiently hydrophilic (when f increases above f_c). The evolution of the effective diffusion coefficient at breakthrough presented in the next section confirms this conclusion.

8. Effective diffusion coefficient and relative permeabilities at breakthrough

The evolution of the effective diffusion coefficient (through-plane coefficient over the whole thickness of the network) at BT as a function of hydrophilic pore fraction is shown in Fig. 8 together with the evolution of the overall saturation. The evolution given by Eq. (5) is also plotted in Fig. 8 and can be seen as overpredicting our results (see the end of Section 6 in this respect). Again, one can first distinguish two main domains. For f below f_c, D_{eff} remains high (of the order of 0.4–0.5D) whereas it decreases steadily up to 0 (which is reached for $f \sim 85\%$) as f increases above f_c. As can be seen from Fig. 8, the maximum value of D_{eff} is obtained for a fully hydrophobic network, i.e. $f = 0$. A local maximum in the evolution of D_{eff} is observed for $f \sim f_c$, right before the beginning of the steady drop above f_c. In summary, these results suggest that the loss in performance due a diminished access of gas to the catalyst layer through the GDL resulting from a change in wettability is only marked when $f > f_c$. Below f_c, the best performance is expected for
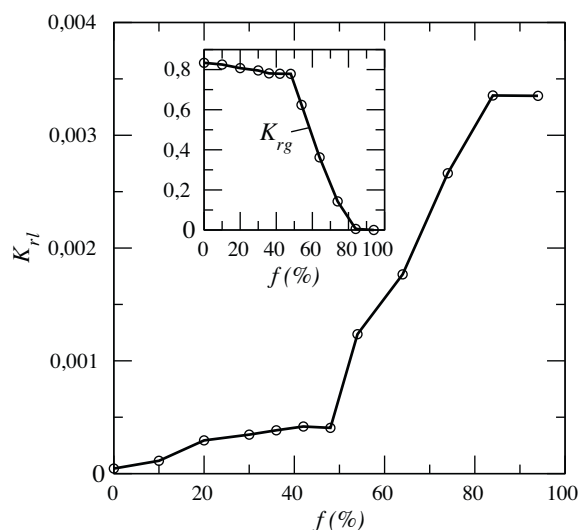
Fig. 9. Evolution of through-plane relative permeabilities at breakthrough as a function of the fraction of hydrophilic pores.

a fully hydrophobic GDL with also good performances expected for f in the range $[0–f_c]$. Of course, these conclusions are for our model GDL. The fact that a GDL becomes or not a mixed wettability system as a result of aging or due to the temperature conditions prevailing in an operating PEMFC remains an open question. Also, even if the mixed wettability assumption is correct, there is no evidence at the moment that the GDL can be considered as a system of purely random wettability as considered in this paper. Nevertheless, our simple model is consistent with the expected effect of a sufficient loss in hydrophobicity and also suggests that a mixed wettability GDL can be an efficient solution as regards the water management problem provided that the hydrophobic fraction of the pore space is sufficiently important. We note that a somewhat similar conclusion was reached in [21].

Similar conclusion can be obtained from the evolution of K_r at breakthrough shown in Fig. 9.

9. Conclusions

In this paper, we explored the effect of a change in wettability from pore network simulations for a model GDL considered as a cubic pore network of random mixed wettability. The study illustrates well the possibilities offered by pore network simulations for establishing the link between a change in the local properties and a change in the macroscopic equilibrium (capillary pressure curve) or transport properties of the porous medium.

The simulations lead to results compatible with the most recent measurements of the water invasion capillary pressure curve for GDLs treated with PTFE. A somewhat surprising result is that the macroscopic properties studied are independent of the fraction of hydrophilic pores and throats in the system as long as this fraction is below a certain threshold corresponding in our model to the percolation threshold of the hydrophilic pore network. This result is somewhat analogous to the experimental results showing that the capillary pressure curve is essentially independent of the PTFE loading as long as the loading is equal to or greater than 5 wt%. Thus it is difficult to infer from the available experimental results concerning the capillary pressure curve of GDLs whether it is more appropriate to consider a GDL as a system of spatially (quasi-) uniform wettability (as suggested from the analysis and results reported in [1] for example) or rather as a system of mixed wettability (i.e. locally hydrophilic in some regions of the pore space and hydrophobic elsewhere).

The same type of question, i.e. a spatially uniform change or on the contrary local changes, is still open as regards the change in wettability that might be due to aging or temperature effect. We explored the option of a change in wettability due to an increase in the fraction of hydrophilic pores and throats, assuming moreover a random distribution of the hydrophilic pores.

This model leads to delineate two main domains, below and above the hydrophilic pore percolation threshold. Below the percolation threshold, all the investigated properties of the system are essentially insensitive to a change in the fraction of hydrophilic pores. Above the percolation threshold, the effect of a change in the fraction of hydrophilic pores becomes quite significant and the gas access through the GDL becomes quite poor when the fraction of hydrophilic pores is high. The identification of these two regimes may help interpret experimental evidences of fuel cell performance loss due to change in wettability.

We note, however, that the other "extreme" scenario, that is a progressive and spatially uniform change in the wettability (leading to water distributions from capillary fingering patterns to compact ones) is difficult to study from pore network simulations at the moment because there is no three-dimensional version of PNM allowing to study accurately the evolution of invasion patterns in the contact angle intermediate range $[70–120°]$ of interest for a GDL. So we do not know if the second scenario of changing uniform wettability would lead to an evolution of the macroscopic properties markedly different from the mixed wettability scenario explored in this paper. Hence, further work on two-phase flow in the intermediate range of contact angle characterizing GDLs is needed.

Finally, we note that the simulations presented in this paper suggest that the best performances can be expected not only with a fully hydrophobic GDL but also with partially hydrophilic GDLs. Hence a partial teflonization of the GDL is not necessarily a problem provided that the GDL contains a sufficient fraction of hydrophobic pores.

Acknowledgements

References

[1] J.D. Fairweather, P. Cheung, D.T. Schwartz, J. Power Sources 195 (2010) 787–793.
[2] L. Cindrella, A.M. Kannan, J.F. Lin, K. Saminathan, Y. Ho, C.W. Lin, J. Wertz, J. Power Sources 194 (2009) 146–160.
[3] O. Chapuis, M. Prat, M. Quintard, E. Chane-Kane, O. Guillot, N. Mayer, J. Power Sources 178 (2008) 258–268.
[4] G.M. Whitesides, P.E. Laibinis, Langmuir 6 (2002) 87–96.
[5] J.T. Gostick, M.A. Ioannidis, M.W. Fowler, M.D. Pritzker, J. Power Sources 194 (2009) 433–444.
[6] P.K. Sinha, P.P. Mukherjee, C.Y. Wang, J. Mater. Chem. 17 (2007) 3089–3103.
[7] A.Z. Weber, R.M. Darling, J. Newman, J. Electrochem. Soc. 151 (2004) A1715–A1727.
[8] R.P. Ramasamy, E.C. Kumbur, M.M. Mench, W. Liu, D. Moore, M. Murthy, Int. J. Hydrogen Energy 33 (2008) 3351–3367.
[9] S. Park, B.N. Popov, Electrochim. Acta 54 (2009) 3473–3479.
[10] R. Borup, J. Meyers, et al., Chem. Rev. 107 (2007) 3904–3951.
[11] C. Lim, C.Y. Wang, Electrochim. Acta 49 (2004) 4149–4156.
[12] Y.M. Vol'fkovich, V.E. Sosenkin, et al., Russ. J. Electrochem. 44 (2008) 278–285.
[13] H. Chraibi, M. Prat, O. Chapuis, Phys. Rev. E 79 (2009) 026313.
[14] L. Hao, P. Cheng, Int. J. Heat Mass Transfer 53 (9–10) (2010) 1908–1913.
[15] H. Dong, M.J. Blunt, Phys. Rev. E 80 (2009) 036307.
[16] V.P. Schulz, J. Becker, A. Wiegmann, P.P. Mukherjee, C.Y. Wang, J. Electrochem. Soc. 154 (4) (2007) B419–B426.
[17] J.T. Gostick, M.A. Ioannidis, M.W. Fowler, M.D. Pritzker, J. Power Sources 173 (2007) 277–290.
[18] K.J. Lee, J.H. Nam, C.J. Kim, Electrochim. Acta 54 (2009) 1166.
[19] B. Markicevic, A. Bazylak, N. Djilali, J. Power Sources 171 (2007) 706–717.

[20] P.K. Sinha, C.Y. Wang, Electrochem. Acta 52 (2007) 7936–7945.
[21] P.K. Sinha, C.Y. Wang, Chem. Eng. Sci. 63 (2008) 1081–1091.
[22] M. Rebai, M. Prat, J. Power Sources 192 (2009) 534–543.
[23] D. Wilkinson, J.F. Willemsen, J. Phys. A: Math. Gen. 16 (1983) 3365–3376.
[24] M.J. Blunt, Soc. Petrol. Eng. J. 2 (1997) 449–510.
[25] M.J. Blunt, J. Petrol. Sci. Eng. 20 (1998) 117–125.
[26] H. Wong, S. Morris, C. Radke, J. Colloid Interface Sci. 148 (1992) 317–336.
[27] O. Chapuis, M. Prat, Phys. Rev. E 75 (2007) 046311.
[28] J.L. Hilden, K.P. Trumble, J. Colloid Interface Sci. 267 (2003) 463–474.
[29] T. Koido, T. Furusawa, K. Moriyama, J. Power Sources 175 (2008) 127–136.
[30] I.S. Hussaini, C.Y. Wang, J. Power Sources 195 (2010) 3830–3840.
[31] N. Zamel, N.G.C. Astrath, X. Li, J. Shen, J. Zhou, F.B.G. Astrath, H. Wang, Z.-S. Liu, Chem. Eng. Sci. (2010), doi:10.1016/j.ces.2009.09.044.
[32] L. Ceballos, M. Prat, J. Power Sources 195 (2010) 825–828.
[33] S. Litster, D. Sinton, N. Djilali, J. Power Sources 154 (2006) 95–105.
[34] D. Stauffer, A. Aharony, Introduction to Percolation Theory, Taylor & Francis, London, 1992.